Clusters of bacterial RNA polymerase are biomolecular condensates that assemble through liquid–liquid phase separation

Anne-Marie Ladouceur[a,1], Baljyot Singh Parmar[b,1], Stefan Biedzinski[a], James Wall[a], S. Graydon Tope[a], David Cohn[a], Albright Kim[a], Nicolas Soubry[a], Rodrigo Reyes-Lamothe[a], and Stephanie C. Weber[a,b,2]

[a]Department of Biology, McGill University, Montreal, QC H3A 1B1, Canada; and [b]Department of Physics, McGill University, Montreal, QC H3A 2T8, Canada

Edited by Richard A. Young, Massachusetts Institute of Technology, Cambridge, MA, and approved June 23, 2020 (received for review March 17, 2020)

Once described as mere "bags of enzymes," bacterial cells are in fact highly organized, with many macromolecules exhibiting nonuniform localization patterns. Yet the physical and biochemical mechanisms that govern this spatial heterogeneity remain largely unknown. Here, we identify liquid–liquid phase separation (LLPS) as a mechanism for organizing clusters of RNA polymerase (RNAP) in *Escherichia coli*. Using fluorescence imaging, we show that RNAP quickly transitions from a dispersed to clustered localization pattern as cells enter log phase in nutrient-rich media. RNAP clusters are sensitive to hexanediol, a chemical that dissolves liquid-like compartments in eukaryotic cells. In addition, we find that the transcription antitermination factor NusA forms droplets in vitro and in vivo, suggesting that it may nucleate RNAP clusters. Finally, we use single-molecule tracking to characterize the dynamics of cluster components. Our results indicate that RNAP and NusA molecules move inside clusters, with mobilities faster than a DNA locus but slower than bulk diffusion through the nucleoid. We conclude that RNAP clusters are biomolecular condensates that assemble through LLPS. This work provides direct evidence for LLPS in bacteria and demonstrates that this process can serve as a mechanism for intracellular organization in prokaryotes and eukaryotes alike.

RNA polymerase | liquid–liquid phase separation | biomolecular condensate | spatial organization | single-molecule tracking

Living cells are divided into functional compartments called organelles. In eukaryotes, lipid membranes create a diffusion barrier between organelles and the cytoplasm, such that each compartment maintains a distinct biochemical composition that is tailored to its function (1). Prokaryotes typically lack internal membranes and instead must use alternate mechanisms for spatial and functional organization. For example, bacterial microcompartments, such as the carboxysome, are surrounded by a selectively permeable protein shell (2). Storage granules also contain a surface layer of proteins (3). In addition to these discrete organelle-like structures, chromosomal loci (4–6), proteins (7, 8), and lipids (9) have all been found to exhibit nonuniform localization patterns in bacteria. However, in most cases, the mechanisms that give rise to such spatial heterogeneity, and its functional significance, remain unclear.

Liquid–liquid phase separation (LLPS) has recently emerged as a novel mechanism for compartmentalization in eukaryotic cells (10). This process mediates the assembly of "biomolecular condensates," an unusual class of organelles that lack delimiting membranes (11). For example, P granules (12) and stress granules (13) consist of local concentrations of protein and RNA, which rapidly assemble in the cytoplasm in response to developmental or environmental changes. The nucleoplasm also undergoes phase separation to generate a variety of "nuclear bodies" (14, 15), including the prominent nucleolus (16, 17). Intriguingly, membraneless bodies have also been described in chloroplasts (18, 19) and mitochondria (20). Given these organelles' endosymbiotic origin (21), these observations raise the possibility that prokaryotes also use LLPS to compartmentalize their cells.

In eukaryotes, LLPS is mediated by proteins containing multivalent domains and disordered regions (22–24) that bring molecules together into dynamic condensates through transient interactions. Sequence analysis predicts that bacterial proteomes have a much lower frequency of disordered regions than eukaryotic proteomes: Only 4.2% compared to 33%, respectively (25). This paucity of disorder raises doubts about the prevalence of LLPS in this domain of life. Nevertheless, recent work suggests that bacteria may indeed contain biomolecular condensates (26). For example, the DEAD-box helicases DeaD, SrmB, and RhlE form foci in *Escherichia coli* (27) and RNase E forms foci in *Caulobacter crescentus* and other α-proteobacteria (28). Moreover, the disordered C-terminal domain of RNase E is necessary and sufficient for foci assembly in vivo.

Despite these observations, direct evidence for LLPS in bacteria is still lacking. This gap arises in part due to the small size of bacteria and the inherent difficulty of analyzing structures near or below the diffraction limit. Yet a more fundamental problem also exists: A lack of consensus criteria to define LLPS in vivo. This is true even in eukaryotic systems, as highlighted by several recent reviews (15, 29, 30).

Significance

Bacterial cells are small and were long thought to have little to no internal structure. However, advances in microscopy have revealed that bacteria do indeed contain subcellular compartments. But how these compartments form has remained a mystery. Recent progress in larger, more complex eukaryotic cells has identified a novel mechanism for intracellular organization known as liquid–liquid phase separation. This process causes certain types of molecules to concentrate within distinct compartments inside the cell. Here, we demonstrate that the same process also occurs in bacteria. This work, together with a growing body of literature, suggests that liquid–liquid phase separation is a common mechanism for intracellular organization in both eukaryotic and prokaryotic cells.

Author contributions: A.-M.L., B.S.P., and S.C.W. designed research; A.-M.L., B.S.P., S.B., J.W., S.G.T., D.C., and A.K. performed research; A.-M.L., B.S.P., N.S., and R.R.-L. contributed new reagents/analytic tools; A.-M.L., B.S.P., S.B., J.W., and S.C.W. analyzed data; and S.C.W. wrote the paper.

The authors declare no competing interest.

This article is a PNAS Direct Submission.

[1]A.-M.L. and B.S.P. contributed equally to this work.

[2]To whom correspondence may be addressed. Email: steph.weber@mcgill.ca.

This article contains supporting information online at https://www.pnas.org/lookup/suppl/doi:10.1073/pnas.2005019117/-/DCSupplemental.

First published July 16, 2020.

To overcome these challenges, we combine traditional chemical and genetic perturbations with single-molecule tracking to investigate the clustering of bacterial RNA polymerase (RNAP). RNAP is distributed throughout the nucleoid in cells grown in minimal media, but concentrates into distinct clusters in cells grown in rich media (31, 32). This nutrient-dependent localization has been well-characterized (33, 34), but the mechanisms that govern RNAP clustering remain unclear (35, 36). Here, we show that clusters of bacterial RNAP are biomolecular condensates. They assemble in a rapid and discontinuous fashion, they are sensitive to hexanediol, and their molecular components are dynamic. Our results demonstrate that bacteria harness LLPS to generate subcellular compartments.

Results

RNAP Clusters during Log Phase in Rich Media. To investigate the mechanisms governing the spatial organization of RNAP in bacterial cells, we generated an *E. coli* strain that expresses an mCherry fusion of the β′ subunit (RpoC) from its endogenous locus. We performed outgrowth experiments by diluting saturated overnight cultures into fresh media at 37 °C. RNAP clusters rapidly disperse when cells are transferred from liquid culture at 37 °C to agarose pads at room temperature (32, 37). To preserve the native subcellular distribution of RNAP, we collected samples at regular time intervals and immediately fixed them in formaldehyde before imaging at room temperature. Fluorescence localization patterns observed in fixed cells were similar to those in live cells when imaged at 37 °C (*SI Appendix*, Fig. S1).

The spatial organization of RNAP depended on the phase of growth. RNAP is dispersed throughout the nucleoid in lag-phase cells (Fig. 1*A*, 0 min). In nutrient-rich media (LB and EZ), RNAP clusters into several bright foci per cell during log phase (Fig. 1*A*, 60 to 180 min) and gradually disperses as cells reenter stationary phase (Fig. 1*A*, 240 to 360 min). In minimal media (M9), RNAP clustering is delayed and less pronounced (Fig. 1*A*, 120 to 300 min). These observations are consistent with previous reports examining log-phase cells grown in rich and minimal media (32–34).

In fast growth conditions, the *E. coli* chromosome undergoes overlapping rounds of replication (38) and folds into a compact

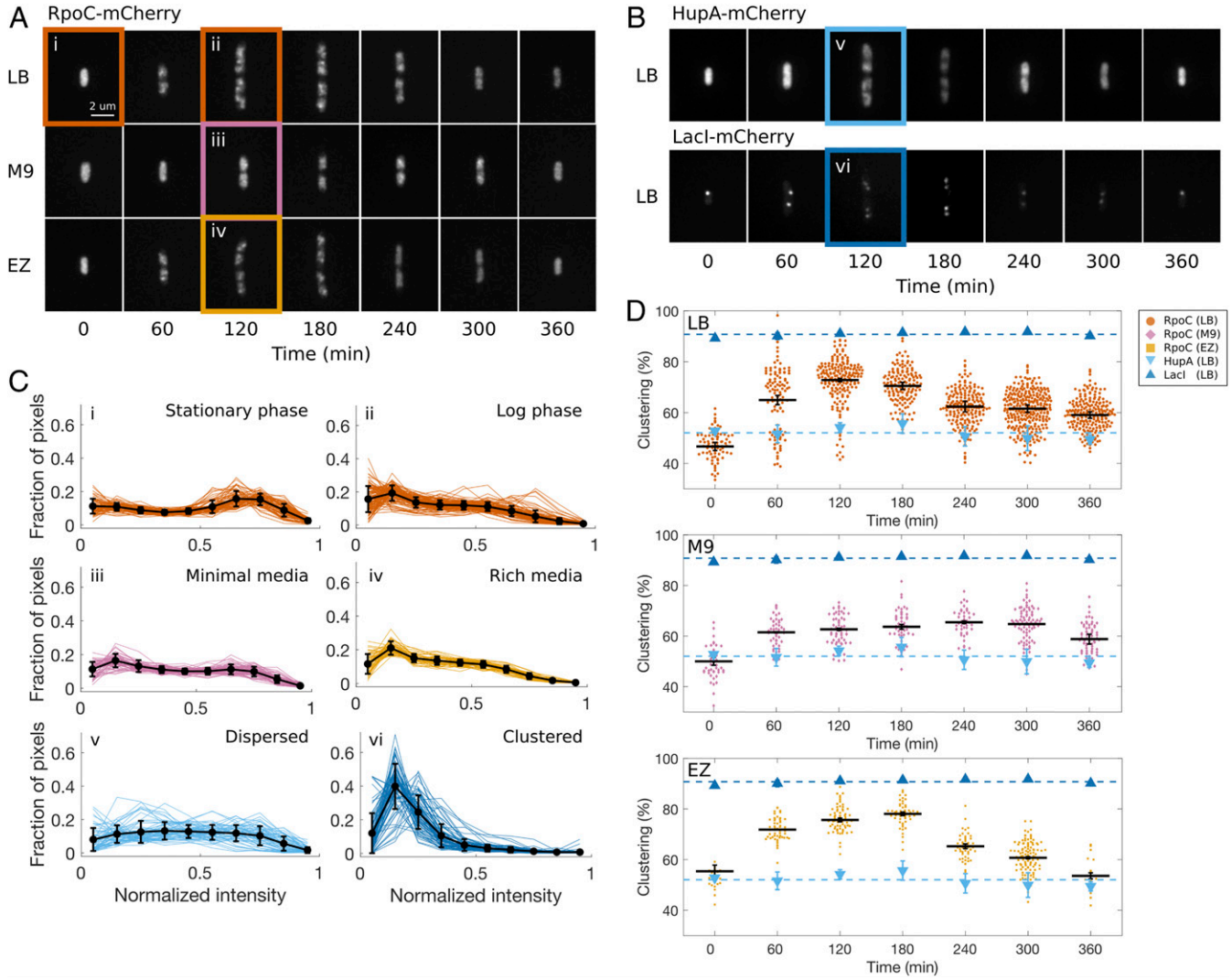

Fig. 1. (*A*) Fluorescence images of fixed cells expressing RpoC-mCherry collected during outgrowth at 37 °C in rich (LB), minimal (M9), or defined (EZ) media. (*B*) Fluorescence images of fixed cells expressing HupA-mCherry or LacI-mCherry collected during outgrowth at 37 °C in LB. (*C*) Normalized pixel intensity histograms for conditions highlighted in *A* and *B*, *i–vi*. (*D*) Clustering of RpoC during outgrowth in LB ($n = 6$), M9 ($n = 3$), and EZ ($n = 3$). Data points correspond to individual cells; black bars represent means, error bars are SEM across n biological replicates. Triangles represent mean ± SEM for HupA and LacI controls ($n = 3$ each). Dashed lines are the means for HupA and LacI across all time points.

filamentous structure (39–41). Since RNAP binds to DNA, the observed clustering may result indirectly from changes in nucleoid morphology during outgrowth. To test this hypothesis, we repeated the outgrowth experiment with a strain expressing an mCherry fusion of HupA (42), a histone-like protein that binds throughout the nucleoid (43). Although the nucleoid becomes more dense in log phase (Fig. 1*B*, 120 to 180 min), we did not observe any distinct foci, suggesting that RNAP clustering is not caused by DNA compaction.

To quantify the spatial distribution of RNAP over time, we adapted a method previously established to monitor chromosome condensation (44) and nucleolar morphology (45). Briefly, individual cells were segmented from brightfield images and the fluorescence intensity per pixel (I) was normalized by the minimum and maximum values in the segmented area, such that $I_n = (I - I_{min})/(I_{max} - I_{min})$. The resulting normalized pixel-intensity histogram shifts from an approximately uniform distribution at 0 min (Fig. 1 *C*, *i*) to a right-skewed distribution at 120 min (Fig. 1 *C*, *ii*). We observed a similar shift from uniform to skewed distribution for log-phase cells in M9 compared to EZ (Fig. 1 *C*, *iii* and *iv*). The shape of the histogram reflects the degree to which RNAP is dispersed or clustered in the cell. For comparison, HupA-mCherry provided a baseline for a dispersed localization pattern (Fig. 1 *C*, *v*), while LacI-mCherry served as a control for a clustered pattern (Fig. 1 *C*, *vi*). The latter strain contains a *lacO* array integrated near the terminus of the chromosome, resulting in one to four copies to which LacI-mCherry binds (Fig. 1*B*).

To compare histograms between individual cells and across different time points and media, we calculated the percent of pixels with a normalized intensity below a threshold, $I_n < 0.5$, for each cell. This percent corresponds to the area segmented as background, which increases upon protein clustering (*SI Appendix*, Fig. S1). In LB, lag-phase cells have 47 ± 2% pixels below the threshold, while log-phase cells have 73 ± 1%, reflecting the transition from a dispersed to clustered organization (Fig. 1 *C* and *D*). Interestingly, this transition appears to be discontinuous. At 60 min, the population is bimodal, with a majority of cells displaying clusters while 30 ± 7% of cells retain the dispersed localization pattern. By 120 min, nearly all cells have assembled clusters (Fig. 1*D*, LB). The discrete transition from dispersed to clustered organization is reminiscent of a first-order phase transition. RNAP also clusters in log-phase cells in M9, although to a lesser extent, and in EZ. The kinetics of clustering differ slightly between LB and EZ (Fig. 1*D*), perhaps due to the distinct nutrient composition of each medium.

RNAP Clustering Is Mediated by Protein–Protein Interactions, not Solely DNA-Binding. Several mechanisms have been proposed to explain RNAP clustering. The most popular is the DNA-binding, or transcription factory, model (Fig. 2*A*). In this model, RNAP clusters are composed of polymerases that are directly bound to DNA and actively transcribing (31, 32). Under fast growth conditions, RNAP is densely packed on *rrn* operons (46) and the vast majority are engaged in synthesis of ribosomal RNA (rRNA) (47), prompting comparisons to the eukaryotic nucleolus (37). However, recent evidence indicates that nucleoid structure may play a more dominant role in RNAP clustering than transcriptional activity itself (36). Alternatively, we hypothesize that RNAP clusters may instead assemble primarily by LLPS such that RNAP is maintained at a high local concentration through weak multivalent protein–protein interactions, independent of its transcriptional activity (Fig. 2*A*).

To distinguish between these models, we treated cells with the aliphatic alcohol 1,6-hexanediol (Hex). This chemical dissolves liquid-like condensates, but not solid-like aggregates, in yeast (48) and mammalian cells (49) and has become a useful, although not definitive, assay for LLPS (50). Consistent with our hypothesis, RNAP clusters rapidly dispersed following addition of Hex to cells grown in LB at 37 °C for 120 min (Fig. 2 *B* and *C*). The effect was dose-dependent and reversible, as RNAP clusters quickly reassembled when the Hex was washed out. Importantly, DNA-bound foci of LacI-mCherry are resistant to Hex (Fig. 2 *B* and *C*), demonstrating that this treatment does not interfere with direct protein–DNA binding. This observation is consistent with results from human cells, in which Hex does not disrupt the sequence-specific binding of LacI to *lacO* (51) or the nonspecific binding of RNA polymerase II to viral DNA (52).

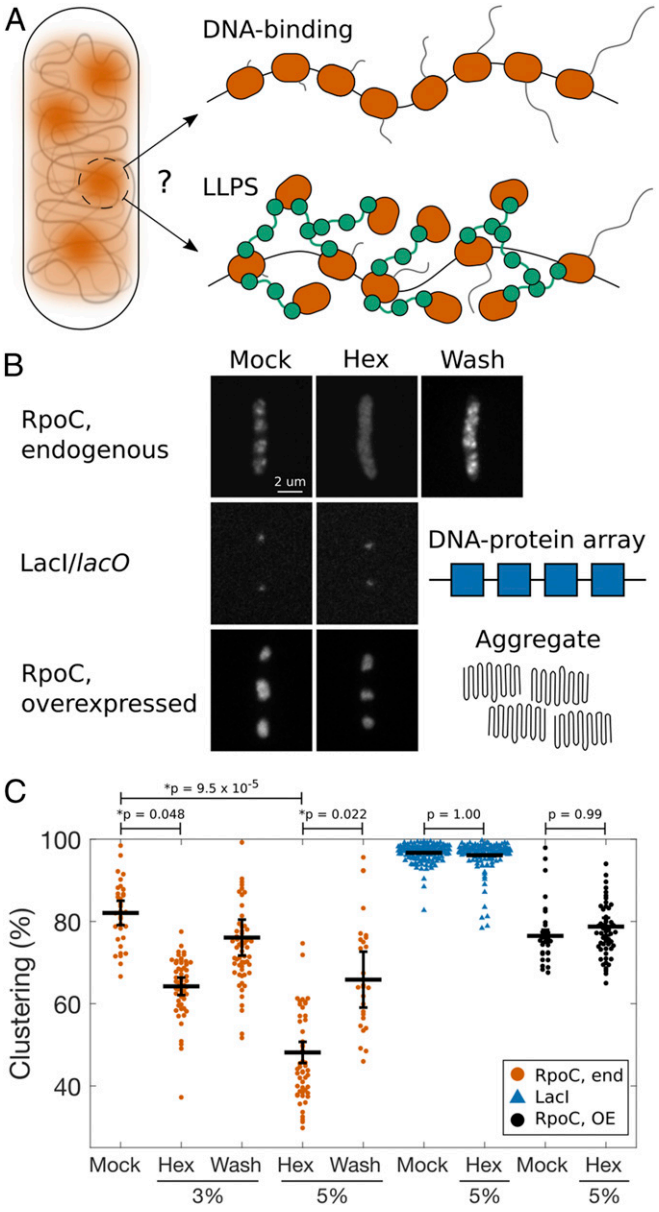

Fig. 2. (*A*) Possible mechanisms for RNAP clustering. The DNA-binding hypothesis proposes that RNAP molecules cluster through direct binding to DNA. Alternatively, RNAP molecules may instead cluster through LLPS. (*B*) Fluorescence images of fixed cells expressing RpoC-mCherry from its native promoter (endogenous), LacI-mCherry, or RpoC-GFP from an IPTG-inducible promoter on a high copy number plasmid. Cells were treated with media (Mock) or 5% Hex for 5 min, and subsequently washed with fresh media to remove Hex (Wash). (*C*) Quantification of clustering of fluorescent proteins for each treatment condition. Data points correspond to individual cells; black bars represent means, error bars are SEM across $n = 3$ biological replicates. *P* values calculated by ANOVA and Tukey–Kramer post hoc test.

Finally, to further validate this assay in bacteria, we used an isopropyl-β-D-thiogalactopyranoside (IPTG)-inducible plasmid to overexpress GFP-RpoC (53). When overexpressed, RpoC accumulates in the cytoplasm, rather than the nucleoid, and forms large aggregates at midcell and the poles. As expected, these aggregates were not affected by Hex treatment (Fig. 2 *B* and *C*). Thus, we find that short (5 min) exposure to Hex selectively disrupts dynamic subcellular compartments in *E. coli*, as in eukaryotes. Together, these results indicate that RNAP clusters are physically and chemically distinct from DNA–protein arrays and protein aggregates. Moreover, they suggest that weak protein–protein interactions contribute to RNAP clustering and that it is not mediated solely by DNA-binding.

Antitermination Factors Are Required for RNAP Clustering. Next, we sought to identify molecular components that are required for RNAP clustering. We began by compiling a list of proteins that contain disordered regions. Among the most highly expressed disordered proteins in *E. coli* are RpoZ, an RNAP subunit; NusA and NusG, antitermination factors that interact directly with RNAP and each other; and H-NS, a nucleoid-associated protein that negatively regulates *rrn* transcription (54). To identify additional candidates, we calculated the mean net charge and mean hydrophobicity for all 4,351 proteins in the *E. coli* proteome (Fig. 3*A*). Previous sequence analyses identified an empirical relationship that distinguishes between folded and natively unfolded proteins based on their amino acid composition (55). Using this classifier, we found 202 proteins, or 4.6% of the proteome, that are likely unfolded. We focused on proteins that are known to be involved in rRNA transcription (Table 1). Of this set, five proteins, or 25%, fall above the unfolded/folded boundary on the charge-hydrophobicity plot (Fig. 3*A* and Table 1). Notably, RpoZ, NusA, and NusG were not identified by this method. Finally, disordered regions in several of these proteins have been confirmed experimentally (56–62). Taking these data together, we find that transcriptional regulators in *E. coli* appear to be enriched for disordered proteins, as they are in eukaryotes (25, 63).

To determine whether candidate proteins contribute to RNAP clustering, we transduced the rpoC-mCherry marker into available mutants from the Keio knockout collection (64). The resulting strains were grown in LB at 37 °C and cells were collected at 120 min, fixed with formaldehyde, and imaged. First, we examined the spatial organization of RNAP in the absence of Fis, a transcriptional activator (65), and Lrp, a transcriptional repressor (66). Fis is a strong candidate for LLPS: Its N-terminal domain is disordered (58) (*SI Appendix*, Fig. S2*B*); it has multiple binding sites upstream of each *rrn* promoter (67); and it is highly expressed during log phase (68), when RNAP clusters assemble (Fig. 1). Moreover, we found that purified GFP-Fis condenses into liquid-like droplets in a salt-dependent manner in vitro (*SI Appendix*, Fig. S3*A*). Unexpectedly, however, deletion of Fis does not impair RNAP clustering, as RpoC-mCherry still assembled into bright foci in Δ*fis* cells (Fig. 3*B*).

Lrp contains a flexible linker that connects folded N- and C-terminal domains (69), but is otherwise ordered (Table 1 and *SI Appendix*, Fig. S2*C*). Therefore, this protein is not expected to phase separate and serves as a negative control. We observed no change in RNAP clustering in Δ*lrp* cells compared to wildtype (WT) (Fig. 3*B*).

NusA and NusG are essential in *E. coli* (70), so we next tested NusB for its role in RNAP clustering. NusB colocalizes with RNAP clusters (71) and, together with NusA, NusG, NusE (the 30S ribosomal protein S10), and SuhB, forms a complex that prevents premature Rho-dependent termination of *rrn* genes (72, 73). When we visualized RpoC-mCherry in the Δ*nusB* strain, we observed a more dispersed localization pattern (Fig. 3*B*). RNAP is distributed throughout the nucleoid of Δ*nusB* cells and concentrates into just a few dim foci. Importantly, although Δ*nusB* cells exhibit a growth defect, they display a lower degree of clustering than observed in WT cells at the same (slower) growth rate (*SI Appendix*, Fig. S2*E*). These results suggest that NusB, or another antitermination factor (Table 1), is required for efficient RNAP clustering.

NusA Undergoes LLPS In Vitro. NusA is an abundant protein composed of six folded domains connected by flexible linkers (Fig. 3*C*). The central S1 motif and two K homology (KH) domains bind RNA (74, 75), while the N-terminal domain and two C-terminal acidic repeat (AR) domains interact with a variety of proteins, including multiple subunits of RNAP (76–78), NusG (79), SuhB (72, 73), and the bacteriophage λ-protein N (80, 81). AR2 can also interact with KH1 to block RNA binding (77, 82). This modular architecture, which facilitates both heterotypic and homotypic interactions, is consistent with the "stickers-and-spacers" model used to describe LLPS (83).

To test its intrinsic ability to phase separate, we purified GFP-NusA and monitored its behavior in vitro using complementary biochemical assays (84, 85). First, we looked for condensed-phase protein droplets by fluorescence microscopy. Second, we measured the protein concentration of NusA solutions following centrifugation. In this latter assay, the final concentration matches the initial concentration when NusA remains dissolved. However, if NusA phase separates, then centrifugation collects the dense phase in the pellet and the (lower) concentration of the supernatant corresponds to the saturation concentration at the phase boundary. We varied the salt concentration in our assay buffer to modulate the affinity of intermolecular interactions and map the phase diagram for NusA.

Initially, we failed to detect phase separation by either technique. NusA remains soluble up to at least 22.5 μM at all salt concentrations tested (25 to 225 mM NaCl) (*SI Appendix*, Fig. S3*B*). To mimic the crowded environment inside a cell, we repeated these assays in the presence of 10% dextran, which has been used to induce phase separation of both prokaryotic and eukaryotic proteins (86, 87). Under these conditions, we consistently observed phase separation and found qualitative and quantitative agreement between the two assays (Fig. 3*D*). In the presence of dextran, GFP-NusA forms large spherical droplets at physiological salt concentrations above a saturation concentration of ∼10 μM. Time-lapse imaging revealed that multiple droplets fuse upon contact, demonstrating liquid-like properties (Fig. 3*E*). Consistent with the dispersal of clusters by Hex in vivo (Fig. 2), we also found that NusA droplets dissolved in 10% Hex in vitro (*SI Appendix*, Fig. S3*C*). These results indicate that NusA is capable of forming homotypic interactions that can drive LLPS. However, as we found for Fis (*SI Appendix*, Fig. S3*A*), they do not necessarily imply that NusA phase separates in vivo.

NusA Nucleates Foci In Vivo. To determine whether NusA can nucleate condensates in cells, we used the *lacO*/LacI system in a strategy similar to that recently applied to eukaryotic transcription factors (51). We generated two constructs—1) LacI-mNeonGreen alone and 2) LacI-NusA-mNeonGreen, which contains the full-length NusA protein—expressed them in cells containing a *lacO* array near the terminus of the chromosome, and counted the number of fluorescent foci in each cell (Fig. 3*F*). Cells expressing LacI-mNG had 1.4 ± 0.2 foci per cell (Fig. 3*G*), consistent with the copy number of the *lacO* array (88). In contrast, cells expressing the NusA fusion protein (LacI-NusA-mNG) had significantly more foci, with 3.9 ± 0.6 per cell (Fig. 3 *F* and *G*). NusA has multiple protein interaction and RNA-binding domains (Fig. 3*C*), but it does not bind DNA directly. Therefore, the excess foci likely assemble through protein–protein or protein–RNA interactions with the NusA fusion protein. Moreover, the LacI-NusA-mNG foci appear larger/brighter than the LacI-mNG foci (Fig. 3*F*), consistent with condensates whose size is determined by protein concentration

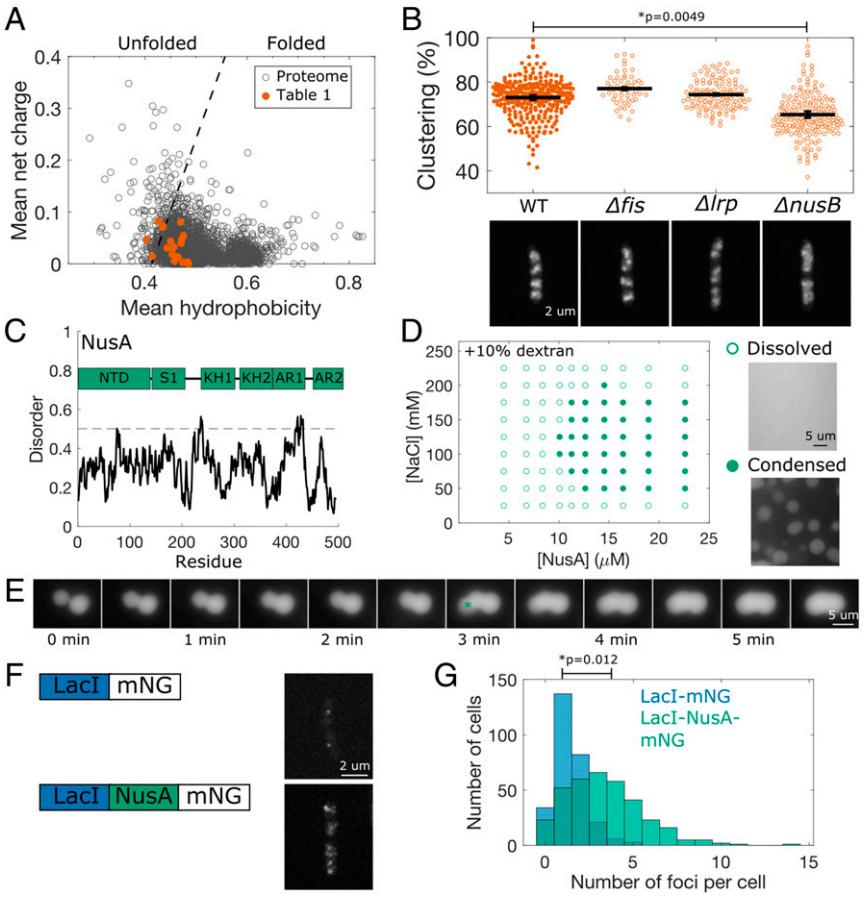

Fig. 3. (*A*) Charge vs. hydrophobicity plot for the *E. coli* proteome, with proteins from Table 1 highlighted. The dashed line represents an empirical border between proteins that are natively unfolded (left) and folded (right). (*B*) Clustering and fluorescence images of WT and deletion mutants expressing RpoC-mCherry. *P* values were calculated by ANOVA and Tukey–Kramer post hoc test. (*C*) Domain structure and predicted disorder (by IUPred) of NusA. (*D*) Phase diagram for purified NusA in the presence of 10% dextran. Open circles indicate conditions in which the protein is dissolved; closed circles indicate conditions in which the protein is condensed. (*E*) Montage of NusA droplet fusion. A third droplet falls from solution at $t = 3$ min (marked by *). (*F*) Fluorescence images of live cells expressing LacI-mNeonGreen or LacI-NusA-mNeonGreen. (*G*) Histogram of number of foci per cell for each protein construct ($n = 3$). *P* value was calculated by unpaired, two-tailed Student's *t* test.

rather than the length of an array of DNA-binding sites. Together, these observations suggest that NusA can phase separate in vivo, independently of specific DNA binding.

Components of RNAP Clusters Are Dynamic. A defining feature of liquid-like condensates is the dynamic behavior of their components, which rearrange within the condensate and exchange with the surrounding bulk phase (15). To investigate the dynamics of RNAP cluster components, we used single-molecule tracking. We generated new strains expressing either RpoC or NusA fused to the photoconvertible protein mMaple3 (89). When maintained at 37 °C, these live cells display a clustered localization pattern of preconverted RpoC-mMaple3, similar to that observed for RpoC-mCherry in fixed cells (*SI Appendix*, Fig. S1). Upon activation with 405-nm light, mMaple3 switches from the green channel to the red, allowing us to visualize single molecules over time (Fig. 4*A*). Using photoactivated localization microscopy (90), we acquired time-lapse movies of live cells growing in EZ medium at 37 °C and tracked the position of RpoC and NusA molecules at 20-ms intervals.

Table 1. Proteins involved in rRNA transcription

RNA polymerase	Transcription factors	Antitermination factors	Ribosomal proteins	Regulators
RpoA	**DksA***,†,‡	**NusA***,†	**S4***,†,‡	RelA
RpoB	**Fis**†	NusB	S10/NusE	SpoT
RpoC	**H-NS***,†,‡	NusE/S10	L3	
RpoD*,‡	Lrp	**NusG***,†	**L4**†	
RpoZ*		SuhB	**L13**†,‡	

Proteins with evidence for disorder are in boldface.
*Evidence for disorder predicted.
†Evidence for disorder experimentally confirmed.
‡Evidence for disorder in Fig. 3*A*.

For both proteins, we observed tracks throughout the nucleoid, with a high density of tracks localized to two to four clusters per cell (Fig. 4*B*). These high-density clusters found in live cells resemble the bright clusters seen in fixed cells (Fig. 1 *A*, *ii*, and *iv*), suggesting that these tracks correspond to molecules inside RNAP clusters. To quantify the mobility of all molecules, we calculated the apparent diffusion coefficient (D_{app}) of each track (*SI Appendix*, *Supplementary Materials and Methods* and Fig. S4*A*). Both RpoC and NusA gave broad distributions, ranging from 5×10^{-3} to 5 $\mu m^2/s$, with an average D_{app} of 0.52 ± 0.01 $\mu m^2/s$ and 0.63 ± 0.01 $\mu m^2/s$, respectively (Fig. 4*C* and Table 2). This wide range of mobilities is similar to previous estimates for RpoC (34, 91) and likely reflects different states of activity, for example molecules engaged in transcription or molecules nonspecifically bound to DNA (91). Interestingly, there appeared to be a correlation between track density and mobility, with molecules in high-density clusters tending to move more slowly than molecules in low-density regions of the nucleoid (Fig. 4*B*).

If clustering were caused by DNA binding, then RNAP molecules in a cluster would have the same mobility as a DNA locus. However, if clustering were instead mediated by LLPS, then RNAP molecules may move differently inside a cluster compared to when actively transcribing DNA or diffusing through the rest of the nucleoid. To measure the baseline mobility of a DNA locus, we tracked LacI-mMaple3 molecules in a strain carrying a *lacO* array (90). We observed tracks in only one or two locations per cell, suggesting that most LacI molecules are stably bound to the DNA array (Fig. 4*B*). Consistent with this interpretation, and with previous measurements of DNA motion in *E. coli* (92), the D_{app} distribution was much narrower for LacI, with a peak near 1×10^{-2} $\mu m^2/s$ (Fig. 4*C*). Moreover, the LacI distribution is shifted left relative to the RpoC and NusA distributions, indicating that the majority of RpoC and NusA

Table 2. Apparent diffusion coefficients ($\mu m^2/s$) from single-molecule tracking

Protein	Class	EZ	M9	Hex
RpoC	ALL	0.52 ± 0.10	0.72 ± 0.04	0.55 ± 0.03
	In	0.16 ± 0.04	0.37 ± 0.05	0.26 ± 0.01
	In/Out	0.44 ± 0.04	0.643 ± 0.003	0.57 ± 0.02
	Out	0.61 ± 0.13	0.81 ± 0.02	0.66 ± 0.04
NusA	ALL	0.63 ± 0.01	0.77 ± 0.02	0.57 ± 0.04
	In	0.18 ± 0.09	0.097 ± 0.003	0.056 ± 0.002
	In/Out	0.47 ± 0.12	0.44 ± 0.03	0.40 ± 0.02
	Out	0.76 ± 0.02	0.85 ± 0.06	0.73 ± 0.05
LacI	ALL	0.11 ± 0.03	0.11 ± 0.02	0.11 ± 0.01
	In	0.023 ± 0.004	0.023 ± 0.002	0.021 ± 0.002
	In/Out	0.65 ± 0.07	0.56 ± 0.05	0.22 ± 0.04
	Out	0.37 ± 0.17	0.32 ± 0.04	0.37 ± 0.06

Values are mean ± SEM across $n = 4$ to 6 biological replicates.

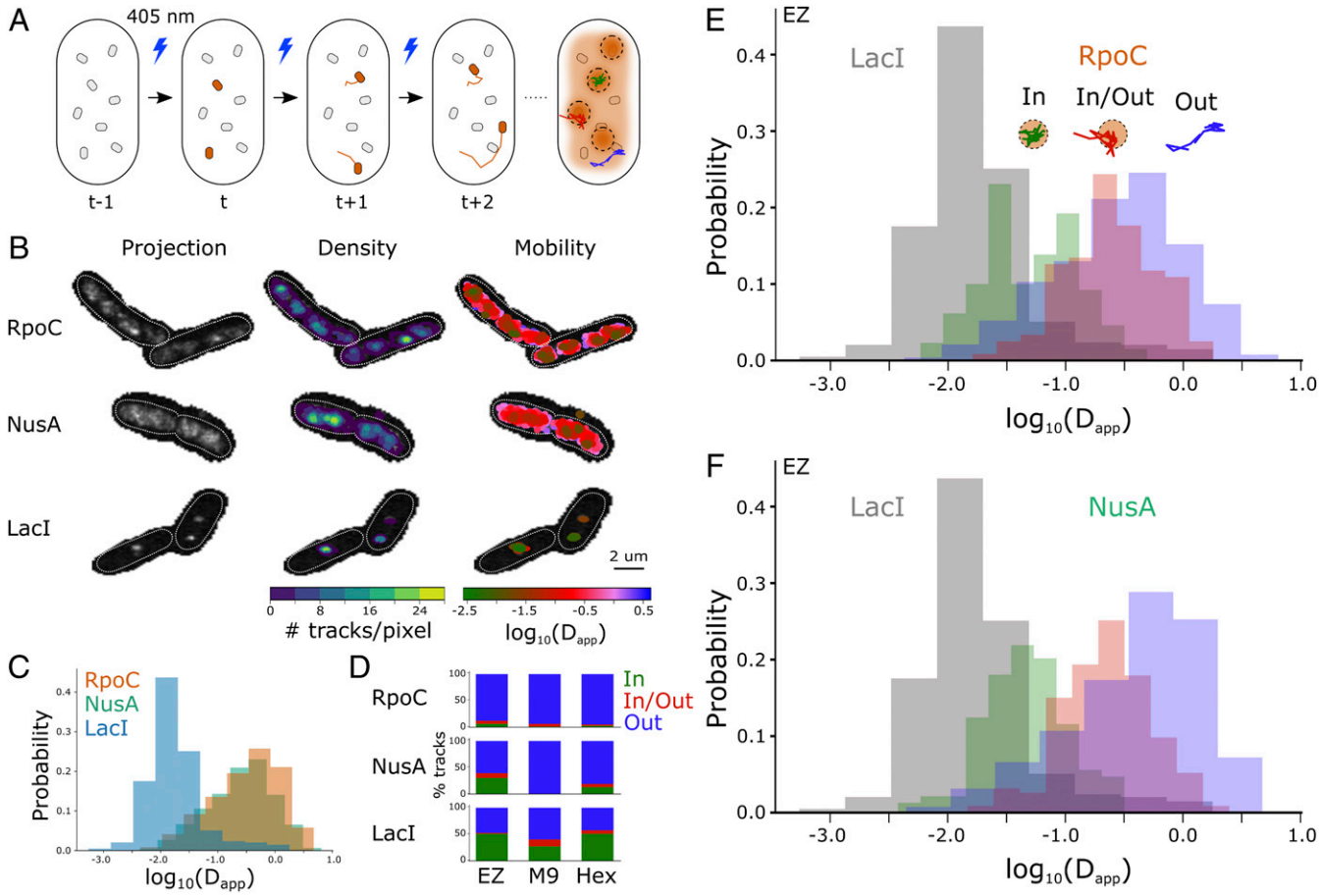

Fig. 4. (*A*) Schematic of a single-molecule tracking experiment. Cells expressing mMaple3 fusion proteins are continuously activated with 405-nm light and converted molecules are tracked over time. (*B*) Maximum-intensity projections of cells expressing RpoC-mMaple3, NusA-mMaple3 or LacI-mMaple3. The density and mobility, respectively, of tracks are overlaid. (*C*) Distribution of D_{app} for all tracks. (*D*) Classification of tracks for each protein under three growth conditions. The In tracks are localized to clusters; In/Out tracks exchange between clusters and the bulk nucleoid; Out tracks do not interact with clusters. (*E*) Distribution of D_{app} for each class of RpoC tracks. (*F*) Distribution of D_{app} for each class of NusA tracks.

molecules move faster than DNA. Nevertheless, there is substantial overlap among the distributions (Fig. 4*C*). The slow-moving RpoC molecules in this overlap region are likely engaged in transcription, while the NusA molecules are engaged in cotranscriptional antitermination. This population of molecules could correspond to all clustered molecules, in support of the DNA-binding model, or only a subset of clustered molecules, in support of the LLPS model (Fig. 2*A*).

To distinguish between these possibilities, and to compare the mobility of molecules in RNAP clusters to the mobility of DNA directly, we developed a stringent classification scheme. First, we created maximum-intensity projections over time to identify regions with a high density of activated molecules (Fig. 4*B*). Second, we defined a "cluster" as any region detected in the projection that overlapped with a minimum of three tracks. Finally, a molecule was designated as "In" if its entire trajectory was contained inside a cluster; "In/Out" if its trajectory crossed a cluster boundary but spent a majority of time points inside a cluster; and "Out" if its trajectory never overlapped with a cluster. This classification scheme is conservative. We intentionally set a strict definition for the In class, preferring to underestimate the number of In molecules in order to calculate their mobility more accurately. As a result, only ~5 to 10% of RpoC tracks and 10 to 30% of NusA tracks were assigned to the In class (Fig. 4*D*). Consequently, the Out class likely contains many false positives, as reflected by the large percentage of molecules assigned to this class (Fig. 4*D*), even for LacI (*SI Appendix*, Fig. S4*B*), and by the leftward skew of the D_{app} distribution for this class (Fig. 4 *E* and *F*).

To validate our classification scheme, we applied two independent methods to the raw (unclassified) data (Fig. 4*C*). First, we used a nonparametric Bayesian approach called single-molecule analysis by unsupervised Gibbs sampling (SMAUG) (93). This method identifies the number of different mobility states in a population of trajectories and calculates the fraction of molecules and apparent diffusion coefficient in each state. Second, we fit a Gaussian mixture model to the full distribution of D_{app} for all tracks. In both cases, we identified three to four subpopulations of molecules with mobilities that are consistent with our results from single-molecule tracking (*SI Appendix*, Fig. S4 *C* and *D*).

After classifying tracks from each strain (Fig. 4*D*), we compared the normalized distributions of D_{app} for each class. RpoC molecules classified as In clusters had a bimodal distribution, with the lower peak overlapping the distribution for LacI (Fig. 4*E*). The higher peak was shifted to the right, centered at ~0.1 $\mu m^2/s$, which is still an order-of-magnitude smaller than the majority of RpoC molecules. These results suggest that RNAP clusters contain two populations of RpoC: One that is bound to DNA and another that is not bound, moves more quickly, and yet remains localized in high-density clusters. We propose that the former population is engaged in transcription, while the latter population is diffusing within a surrounding liquid-like condensate. In addition, the distribution for In/Out molecules overlapped with this high-mobility In population and also extended to much greater values of D_{app}. This is consistent with molecules that are exchanging between a condensed phase and the bulk nucleoid, and which spend variable amounts of time in each phase. Finally, the Out distribution was shifted farthest right, to a mean of 0.61 ± 0.1 $\mu m^2/s$ (Table 2). The high mobility of these molecules suggests that they are diffusing freely through the cytoplasm and nonspecifically bound to the nucleoid. The long, left tail of this distribution likely arises from the misclassification of tracks whose clusters were not detected. Alternatively, some molecules in this tail may be engaged in transcription at other sites throughout the nucleoid.

NusA exhibited similar dynamics (Table 2). Like RpoC, the D_{app} distribution for the In class of NusA partially overlapped with LacI (Fig. 4*F*), indicating that some NusA molecules are likely associated with DNA [presumably indirectly through interactions with RNAP (76, 77)]. Importantly, this class also contains faster-moving molecules, consistent with the LLPS hypothesis. The In/Out and Out distributions are shifted progressively to the right, with mean values comparable to RpoC (Table 2). These data reveal that, like RpoC, NusA exists in several different states in the cell, such that its mobility varies both in space and with molecular density.

Finally, we determined how the dynamics of RpoC and NusA change under different growth conditions. We repeated single-molecule tracking in live cells grown in M9 or in EZ after treatment with 5% Hex. As expected, the percent of tracks that were classified as In clusters decreased in both conditions (Fig. 4*D*), consistent with the reduced RNAP clustering seen in fixed cells (Figs. 1 *A* and *D* and 2 *B* and *C*), as well as the dissolution of NusA droplets in the presence of Hex in vitro (*SI Appendix*, Fig. S3). Furthermore, while the mobility of DNA-bound LacI did not change, the few RpoC molecules that remained in clusters appeared less constrained (Table 2 and *SI Appendix*, Fig. S5). This may be due to changes in the composition or molecular density of the condensates, which could affect their viscosity. Conversely, the mobility of NusA molecules in clusters became more restricted, approaching the motion of a DNA locus. Together, these results suggest that when clusters dissolve in M9 or Hex, NusA disperses into the cytoplasm while RNAP stays localized through transient and nonspecific binding to DNA.

Discussion

Our results demonstrate that RNAP clusters are biomolecular condensates that assemble through LLPS. We found that clustering occurs rapidly during outgrowth in rich media, when cells transition from lag phase to log phase (Fig. 1). We showed that RNAP clusters, but not protein bound to DNA arrays or protein aggregates, dissolve upon treatment with Hex (Fig. 2). This sensitivity is dose-dependent and reversible, suggesting that Hex acts as a solvent to disrupt the intermolecular interactions driving LLPS. We identified NusA as a potential mediator of these interactions (Fig. 3), although additional components may be involved. Deletion of NusB, a component of the antitermination complex, perturbs clustering in cells, while NusA phase separates in vitro and nucleates foci in vivo. Finally, we demonstrated that molecules inside RNAP clusters are dynamic, moving more quickly than DNA loci but more slowly than molecules in the bulk nucleoid (Fig. 4). Together, these results provide direct evidence for the LLPS hypothesis, establishing LLPS as a mechanism for intracellular organization in bacteria.

Our work has important implications for transcriptional regulation in particular and bacterial cell biology in general. It also highlights single-molecule tracking as a powerful tool for examining LLPS in bacteria and beyond.

Partitioning of RNAP. Early biochemical work established that the macromolecular composition of *E. coli* cells varies with growth rate (94, 95). In particular, the total number of RNAPs increases with growth rate, and active RNAPs redistribute from protein-coding genes to stable RNA (i.e., rRNA and tRNA) genes as doubling-time decreases (47). These data were used as support for the DNA-binding model when RNAP clusters were first observed by microscopy (31, 32). They also inspired the development of theoretical models to predict how RNAP is partitioned among various states, such as active transcription of mRNA or rRNA, nonspecific binding to the nucleoid, or free diffusion in the cytoplasm (96, 97).

More recent single-molecule tracking studies assigned RNAP to different states based on its mobility (34, 91). For example, slow-moving molecules ($D < 0.03$ $\mu m^2/s$) were classified as

transcribing, fast-moving molecules (D = 0.7 μm^2/s) as freely diffusing, and molecules with intermediate mobility (D = 0.21 μm^2/s) as binding nonspecifically to the nucleoid (91). The D_{app} values presented in Fig. 4 are comparable to these previous measurements, but our interpretation differs. Instead of assigning all slow-moving molecules to the active transcription state, we favor dividing this group of molecules into two distinct states and introducing an additional "condensed but nontranscribing" state.

Our partitioning scheme is not only consistent with the LLPS hypothesis, it also resolves a discrepancy in the literature. Numerical results (97) agree with gene-expression data (98) but not with single-molecule tracking (91). Specifically, Klumpp and Hwa (97) predicted that ∼21% of RNAP is actively transcribing at a doubling-time of 40 min, while Bakshi et al. (91) estimated 49%. If the updated number of transcribing RNAP were plugged back into Klumpp and Hwa's (97) model, then it would overestimate Nomura et al.'s expression data (98). However, if ∼30% of the slow-moving molecules that Bakshi et al. (91) classified as "transcribing" were not actually transcribing, then the numerical, expression and single-molecule results would be consistent. An alternative interpretation for this discrepancy is that the mRNA elongation rate is slower than assumed in the model.

Transcriptional Regulation. RNAP clusters assemble under fast growth conditions, where rRNA synthesis accounts for ∼80 to 90% of cellular transcription (47). This correlation between clustering and rRNA transcription prompted early comparisons to the eukaryotic nucleolus (31, 32). The nucleolus is a biomolecular condensate composed of immiscible liquid phases that spatiotemporally coordinate ribosome biogenesis at rDNA sites (16, 99–101). By analogy, bacterial RNAP clusters were thought to colocalize with *rrn* operons and function in rRNA synthesis. Indeed, RNAP clusters were recently shown to colocalize with nascent pre-rRNA, confirming that at least some RNAPs within clusters are actively transcribing rRNA (36). Surprisingly, however, this study also found that RNAP clusters persisted even when rRNA transcription was perturbed. These results contradict expectations for the DNA-binding model, but are fully consistent with an LLPS model in which phase separation is mediated primarily by protein–protein interactions, rather than RNA–protein interactions. Furthermore, the size of RNAP clusters is smaller after disruption of rRNA transcription (36). This behavior is similar to the nucleolus, which is stabilized by rRNA, but whose protein components nevertheless condense into small droplets in the absence of rRNA transcription in early *Caenorhabditis elegans* embryos (17).

Ribosome content is limiting for growth, such that bacteria must allocate considerable cellular resources toward ribosome synthesis (102). Thus, it may at first seem wasteful for cells to partition a large fraction of RNAP into a condensed, nontranscribing state. However, a simple calculation (see below) suggests that this state does not compete with the actively transcribing state. In fact, the condensed pool of RNAPs may serve to accelerate reinitiation rates in order to maintain a maximal level of rRNA transcription. *E. coli* has seven *rrn* operons, with four positioned near the origin of replication, such that there are up to 50 copies per cell under optimal growth conditions (37). Each operon is 5.5-kb long, with RNAPs spaced every ∼85 bp (46). Altogether, if every *rrn* is fully saturated with RNAPs, then 50 *rrn*/cell × 5.5 kb/*rrn* × 1 RNAP/85 bp = 3,235 RNAPs are expected to be in the transcribing state. Yet this fraction represents just one-third of the ∼10,000 RNAPs (47), leaving more than enough to populate the condensed, mRNA-transcribing, nonspecifically bound, and freely diffusing states. Furthermore, these estimates are consistent with Klumpp and Hwa's numerical model (97), as well as previous single-molecule studies. PALM analyses conducted at slower growth rates (31- to 73-min doubling-times) counted between 70 and 500 molecules per cluster and 2 to 4 clusters per cell (33, 34, 36), of a total of ∼5,000 RNAPs per cell. Therefore, at both fast and intermediate growth conditions, less than half of all RNAPs are engaged in rRNA transcription and we propose that some of the nontranscribing pool is partitioned into condensates.

LLPS provides a versatile mechanism for cells to control the localization, accessibility, and activity of macromolecules in response to internal and external cues (103, 104). Here, we have shown that *E. coli* harnesses LLPS to reorganize its transcriptional machinery in response to nutrient availability. Further investigations will be necessary to dissect how known transcriptional regulation pathways, including DksA and (p)ppGpp (105), affect the propensity of NusA and other molecular candidates to phase separate, and how clustering influences transcription and subsequent processing of rRNA (106).

Biomolecular Condensates in Bacteria. In addition to RNAP clusters, bacteria likely contain a variety of biomolecular condensates. Many candidates have already been identified. For example, RNase E assembles into bacterial RNP bodies, which are required for efficient mRNA turnover and confer tolerance to stress in *Caulobacter* (28). Several DEAD-box RNA helicases have been proposed to form condensates in *E. coli* (27, 107), but further investigations are necessary to determine whether they undergo LLPS at endogenous expression levels. Polyphosphate granules are another promising candidate. These spherical structures are synthesized during nitrogen starvation in *Pseudomonas* and appear to nucleate, grow, and ripen like liquid droplets (108). In stationary phase, Dps compacts the *E. coli* nucleoid into a dense crystalline-like structure that excludes restriction enzymes yet permits access to RNAP (109). LLPS may also occur on the bacterial membrane, as the ABC transporter Rv1747 phase separates in vitro and forms clusters in *Mycobacterium* (110). There is also in vitro evidence that FtsZ and SlmA may form condensates that regulate the positioning of Z-ring assembly during *E. coli* cell division (86). Together, this growing list of putative condensates suggests that LLPS is ubiquitous in bacteria. These examples span many distantly related species, they appear in all phases of growth (i.e., lag, log, stationary), and they are associated with diverse cellular processes, from gene expression and metabolism to dormancy.

Single-Molecule Tracking as a Tool for Examining LLPS In Vivo. Despite this exciting progress, it remains challenging to study phase separation in any organism but particularly in bacteria. Indeed, while the appearance of fluorescent foci in cells is promising, this alone is not compelling evidence for LLPS because foci can form through many alternative mechanisms (52). So additional tools for interrogating putative condensates are urgently needed. Fluorescence recovery after photobleaching (FRAP) is one of the most commonly used tools, as it can probe both the dynamic rearrangement of molecules within a condensed phase and their rapid exchange with the surrounding environment (14). However, concerns about the liberal interpretation of this method have recently been raised (29). Furthermore, FRAP cannot easily be applied to the submicron structures in bacteria, nor can shape or fusion analysis (99).

Fortunately, single-molecule tracking has recently emerged as a powerful tool for examining LLPS in vivo (52, 111, 112). Indeed, the strongest evidence for bacterial condensates to date comes from single-molecule tracking of proteins in polar microdomains in *Caulobacter* (113). This study revealed that PopZ imposes a diffusion barrier to cytosolic proteins and restricts the mobility of signaling molecules at the cell poles. Our analysis of RNAP mobility (Fig. 4) further underscores the promise of applying single-molecule tracking to characterize the physical properties and functional consequences of biomolecular condensates in bacteria.

In summary, we have identified a biomolecular condensate in *E. coli*. Future work will clarify the molecular components and

interactions that drive assembly of RNAP clusters, and determine how they affect gene expression, ribosome biogenesis, and cell growth and size.

Materials and Methods

All bacterial strains, plasmids, growth conditions, imaging conditions, and data analysis methods used in this study are described in *SI Appendix*.

Data Availability. Bacterial strains and plasmids are available upon request. Single-molecule tracking and data analysis were performed using TrackMate software, which is publicly available (114).

ACKNOWLEDGMENTS. We thank Paul Francois, Jie Xiao, Rick Gourse, Jared Schrader, and Lisa Racki for thoughtful discussions, and members of the S.C.W. and R.R.-L. laboratories for critical reading of the manuscript. Strain SS6282 was a generous gift from Steven Sandler (University of Massachusetts, Amherst). The ASKA library was purchased from the National BioResource Project at the National Institute of Genetics (Japan). Deletion strains from the Keio collection were obtained from the *Escherichia coli* Genetic Stock Center, which is supported by the NSF (DBI-0742708). This work was supported by the Natural Sciences and Engineering Research Council of Canada RGPIN-2017-04435 (to S.C.W.). A.-M.L. was supported by the Fonds de Recherche du Québec–Nature et Technologies (B3X-209443).

1. R. Heald, O. Cohen-Fix, Morphology and function of membrane-bound organelles. *Curr. Opin. Cell Biol.* **26**, 79–86 (2014).
2. M. Sutter, B. Greber, C. Aussignargues, C. A. Kerfeld, Assembly principles and structure of a 6.5-MDa bacterial microcompartment shell. *Science* **356**, 1293–1297 (2017).
3. S. Bresan *et al*., Polyhydroxyalkanoate (PHA) granules have no phospholipids. *Sci. Rep.* **6**, 26612 (2016).
4. P. H. Viollier *et al*., Rapid and sequential movement of individual chromosomal loci to specific subcellular locations during bacterial DNA replication. *Proc. Natl. Acad. Sci. U.S.A.* **101**, 9257–9262 (2004).
5. X. Wang, X. Liu, C. Possoz, D. J. Sherratt, The two *Escherichia coli* chromosome arms locate to separate cell halves. *Genes Dev.* **20**, 1727–1731 (2006).
6. H. J. Nielsen, J. R. Ottesen, B. Youngren, S. J. Austin, F. G. Hansen, The *Escherichia coli* chromosome is organized with the left and right chromosome arms in separate cell halves. *Mol. Microbiol.* **62**, 331–338 (2006).
7. J. N. Werner *et al*., Quantitative genome-scale analysis of protein localization in an asymmetric bacterium. *Proc. Natl. Acad. Sci. U.S.A.* **106**, 7858–7863 (2009).
8. N. J. Kuwada, B. Traxler, P. A. Wiggins, Genome-scale quantitative characterization of bacterial protein localization dynamics throughout the cell cycle. *Mol. Microbiol.* **95**, 64–79 (2015).
9. L. D. Renner, D. B. Weibel, Cardiolipin microdomains localize to negatively curved regions of *Escherichia coli* membranes. *Proc. Natl. Acad. Sci. U.S.A.* **108**, 6264–6269 (2011).
10. Y. Shin, C. P. Brangwynne, Liquid-phase condensation in cell physiology and disease. *Science* **357**, eaaf4382 (2017).
11. S. F. Banani, H. O. Lee, A. A. Hyman, M. K. Rosen, Biomolecular condensates: Organizers of cellular biochemistry. *Nat. Rev. Mol. Cell Biol.* **18**, 285–298 (2017).
12. C. P. Brangwynne *et al*., Germline P granules are liquid droplets that localize by controlled dissolution/condensation. *Science* **324**, 1729–1732 (2009).
13. A. Molliex *et al*., Phase separation by low complexity domains promotes stress granule assembly and drives pathological fibrillization. *Cell* **163**, 123–133 (2015).
14. S. C. Weber, Sequence-encoded material properties dictate the structure and function of nuclear bodies. *Curr. Opin. Cell Biol.* **46**, 62–71 (2017).
15. A. Peng, S. C. Weber, Evidence for and against liquid-liquid phase separation in the nucleus. *Noncoding RNA* **5**, 50 (2019).
16. S. C. Weber, C. P. Brangwynne, Inverse size scaling of the nucleolus by a concentration-dependent phase transition. *Curr. Biol.* **25**, 641–646 (2015).
17. J. Berry, S. C. Weber, N. Vaidya, M. Haataja, C. P. Brangwynne, RNA transcription modulates phase transition-driven nuclear body assembly. *Proc. Natl. Acad. Sci. U.S.A.* **112**, E5237–E5245 (2015).
18. J. Uniacke, W. Zerges, Stress induces the assembly of RNA granules in the chloroplast of *Chlamydomonas reinhardtii*. *J. Cell Biol.* **182**, 641–646 (2008).
19. E. S. Freeman Rosenzweig *et al*., The eukaryotic CO_2-concentrating organelle is liquid-like and exhibits dynamic reorganization. *Cell* **171**, 148–162.e19 (2017).
20. H. Antonicka, F. Sasarman, T. Nishimura, V. Paupe, E. A. Shoubridge, The mitochondrial RNA-binding protein GRSF1 localizes to RNA granules and is required for posttranscriptional mitochondrial gene expression. *Cell Metab.* **17**, 386–398 (2013).
21. V. Zimorski, C. Ku, W. F. Martin, S. B. Gould, Endosymbiotic theory for organelle origins. *Curr. Opin. Microbiol.* **22**, 38–48 (2014).
22. P. Li *et al*., Phase transitions in the assembly of multivalent signalling proteins. *Nature* **483**, 336–340 (2012).
23. M. Kato *et al*., Cell-free formation of RNA granules: Low complexity sequence domains form dynamic fibers within hydrogels. *Cell* **149**, 753–767 (2012).
24. S. C. Weber, C. P. Brangwynne, Getting RNA and protein in phase. *Cell* **149**, 1188–1191 (2012).
25. J. J. Ward, J. S. Sodhi, L. J. McGuffin, B. F. Buxton, D. T. Jones, Prediction and functional analysis of native disorder in proteins from the three kingdoms of life. *J. Mol. Biol.* **337**, 635–645 (2004).
26. E. A. Abbondanzieri, A. S. Meyer, More than just a phase: The search for membraneless organelles in the bacterial cytoplasm. *Curr. Genet.* **65**, 691–694 (2019).
27. M. Hondele *et al*., DEAD-box ATPases are global regulators of phase-separated organelles. *Nature* **573**, 144–148 (2019).
28. N. Al-Husini, D. T. Tomares, O. Bitar, W. S. Childers, J. M. Schrader, α-Proteobacterial RNA degradosomes assemble liquid-liquid phase-separated RNP bodies. *Mol. Cell* **71**, 1027–1039.e14 (2018).
29. D. T. McSwiggen, M. Mir, X. Darzacq, R. Tjian, Evaluating phase separation in live cells: Diagnosis, caveats, and functional consequences. *Genes Dev.* **33**, 1619–1634 (2019).
30. M. Mir, W. Bickmore, E. E. M. Furlong, G. Narlikar, Chromatin topology, condensates and gene regulation: Shifting paradigms or just a phase? *Development* **146**, dev182766 (2019).
31. P. J. Lewis, S. D. Thaker, J. Errington, Compartmentalization of transcription and translation in *Bacillus subtilis*. *EMBO J.* **19**, 710–718 (2000).
32. J. E. Cabrera, D. J. Jin, The distribution of RNA polymerase in *Escherichia coli* is dynamic and sensitive to environmental cues. *Mol. Microbiol.* **50**, 1493–1505 (2003).
33. U. Endesfelder *et al*., Multiscale spatial organization of RNA polymerase in *Escherichia coli*. *Biophys. J.* **105**, 172–181 (2013).
34. M. Stracy *et al*., Live-cell superresolution microscopy reveals the organization of RNA polymerase in the bacterial nucleoid. *Proc. Natl. Acad. Sci. U.S.A.* **112**, E4390–E4399 (2015).
35. T. Gaal *et al*., Colocalization of distant chromosomal loci in space in *E. coli*: A bacterial nucleolus. *Genes Dev.* **30**, 2272–2285 (2016).
36. X. Weng *et al*., Spatial organization of RNA polymerase and its relationship with transcription in *Escherichia coli*. *Proc. Natl. Acad. Sci. U.S.A.* **116**, 20115–20123 (2019).
37. D. J. Jin, C. Cagliero, C. M. Martin, J. Izard, Y. N. Zhou, The dynamic nature and territory of transcriptional machinery in the bacterial chromosome. *Front. Microbiol.* **6**, 497 (2015).
38. R. Reyes-Lamothe, D. J. Sherratt, The bacterial cell cycle, chromosome inheritance and cell growth. *Nat. Rev. Microbiol.* **17**, 467–478 (2019).
39. P. A. Wiggins, K. C. Cheveralls, J. S. Martin, R. Lintner, J. Kondev, Strong intranucleoid interactions organize the *Escherichia coli* chromosome into a nucleoid filament. *Proc. Natl. Acad. Sci. U.S.A.* **107**, 4991–4995 (2010).
40. N. Hadizadeh Yazdi, C. C. Guet, R. C. Johnson, J. F. Marko, Variation of the folding and dynamics of the *Escherichia coli* chromosome with growth conditions. *Mol. Microbiol.* **86**, 1318–1333 (2012).
41. J. K. Fisher *et al*., Four-dimensional imaging of *E. coli* nucleoid organization and dynamics in living cells. *Cell* **153**, 882–895 (2013).
42. A. H. Marceau *et al*., Structure of the SSB-DNA polymerase III interface and its role in DNA replication. *EMBO J.* **30**, 4236–4247 (2011).
43. M. Wery, C. L. Woldringh, J. Rouviere-Yaniv, HU-GFP and DAPI co-localize on the *Escherichia coli* nucleoid. *Biochimie* **83**, 193–200 (2001).
44. P. S. Maddox, N. Portier, A. Desai, K. Oegema, Molecular analysis of mitotic chromosome condensation using a quantitative time-resolved fluorescence microscopy assay. *Proc. Natl. Acad. Sci. U.S.A.* **103**, 15097–15102 (2006).
45. C. Hult *et al*., Enrichment of dynamic chromosomal crosslinks drive phase separation of the nucleolus. *Nucleic Acids Res.* **45**, 11159–11173 (2017).
46. S. L. French, O. L. Miller Jr., Transcription mapping of the *Escherichia coli* chromosome by electron microscopy. *J. Bacteriol.* **171**, 4207–4216 (1989).
47. H. Bremer, P. P. Dennis, Modulation of chemical composition and other parameters of the cell at different exponential growth rates. *Ecosal Plus* **3** (2008).
48. S. Kroschwald *et al*., Promiscuous interactions and protein disaggregases determine the material state of stress-inducible RNP granules. *eLife* **4**, e06807 (2015).
49. Y. Lin *et al*., Toxic PR poly-dipeptides encoded by the C9orf72 repeat expansion target LC domain polymers. *Cell* **167**, 789–802.e12 (2016).
50. S. Kroschwald, S. Maharana, A. Simon, Hexanediol: A chemical probe to investigate the material properties of membrane-less compartments. *Matters* **3**, e201702000010 (2017).
51. S. Chong *et al*., Imaging dynamic and selective low-complexity domain interactions that control gene transcription. *Science* **361**, eaar2555 (2018).
52. D. T. McSwiggen *et al*., Evidence for DNA-mediated nuclear compartmentalization distinct from phase separation. *eLife* **8**, 2503 (2019).
53. M. Kitagawa *et al*., Complete set of ORF clones of *Escherichia coli* ASKA library (a complete set of *E. coli* K-12 ORF archive): Unique resources for biological research. *DNA Res.* **12**, 291–299 (2005).
54. O. Paliy, S. M. Gargac, Y. Cheng, V. N. Uversky, A. K. Dunker, Protein disorder is positively correlated with gene expression in *Escherichia coli*. *J. Proteome Res.* **7**, 2234–2245 (2008).
55. V. N. Uversky, J. R. Gillespie, A. L. Fink, Why are "natively unfolded" proteins unstructured under physiologic conditions? *Proteins* **41**, 415–427 (2000).
56. E. W. Sayers, R. B. Gerstner, D. E. Draper, D. A. Torchia, Structural preordering in the N-terminal region of ribosomal protein S4 revealed by heteronuclear NMR spectroscopy. *Biochemistry* **39**, 13602–13613 (2000).
57. C. P. Smyth *et al*., Oligomerization of the chromatin-structuring protein H-NS. *Mol. Microbiol.* **36**, 962–972 (2000).
58. Y.-S. Cheng, W.-Z. Yang, R. C. Johnson, H. S. Yuan, Structural analysis of the transcriptional activation region on Fis: Crystal structures of six Fis mutants with different activation properties. *J. Mol. Biol.* **302**, 1139–1151 (2000).

59. M. Worbs, R. Huber, M. C. Wahl, Crystal structure of ribosomal protein L4 shows RNA-binding sites for ribosome incorporation and feedback control of the S10 operon. *EMBO J.* **19**, 807–818 (2000).
60. T. Steiner, J. T. Kaiser, S. Marinkoviç, R. Huber, M. C. Wahl, Crystal structures of transcription factor NusG in light of its nucleic acid- and protein-binding activities. *EMBO J.* **21**, 4641–4653 (2002).
61. A. Peredering *et al*., Regulation through the secondary channel–Structural framework for ppGpp-DksA synergism during transcription. *Cell* **118**, 297–309 (2004).
62. Y. Timsit, Z. Acosta, F. Allemand, C. Chiaruttini, M. Springer, The role of disordered ribosomal protein extensions in the early steps of eubacterial 50 S ribosomal subunit assembly. *Int. J. Mol. Sci.* **10**, 817–834 (2009).
63. J. Liu *et al*., Intrinsic disorder in transcription factors. *Biochemistry* **45**, 6873–6888 (2006).
64. T. Baba *et al*., Construction of Escherichia coli K-12 in-frame, single-gene knockout mutants: the Keio collection. *Mol. Syst. Biol.* **2**, 2006.0008 (2006).
65. A. J. Bokal 4th, W. Ross, R. L. Gourse, The transcriptional activator protein FIS: DNA interactions and cooperative interactions with RNA polymerase at the Escherichia coli rrnB P1 promoter. *J. Mol. Biol.* **245**, 197–207 (1995).
66. U. Pul *et al*., LRP and H-NS—Cooperative partners for transcription regulation at *Escherichia coli* rRNA promoters. *Mol. Microbiol.* **58**, 864–876 (2005).
67. C. A. Hirvonen *et al*., Contributions of UP elements and the transcription factor FIS to expression from the seven *rrn* P1 promoters in *Escherichia coli*. *J. Bacteriol.* **183**, 6305–6314 (2001).
68. J. A. Appleman, W. Ross, J. Salomon, R. L. Gourse, Activation of *Escherichia coli* rRNA transcription by FIS during a growth cycle. *J. Bacteriol.* **180**, 1525–1532 (1998).
69. S. de los Rios, J. J. Perona, Structure of the *Escherichia coli* leucine-responsive regulatory protein Lrp reveals a novel octameric assembly. *J. Mol. Biol.* **366**, 1589–1602 (2007).
70. M. Bubunenko, T. Baker, D. L. Court, Essentiality of ribosomal and transcription antitermination proteins analyzed by systematic gene replacement in *Escherichia coli*. *J. Bacteriol.* **189**, 2844–2853 (2007).
71. C. Cagliero, Y. N. Zhou, D. J. Jin, Spatial organization of transcription machinery and its segregation from the replisome in fast-growing bacterial cells. *Nucleic Acids Res.* **42**, 13696–13705 (2014).
72. Y.-H. Huang, N. Said, B. Loll, M. C. Wahl, Structural basis for the function of SuhB as a transcription factor in ribosomal RNA synthesis. *Nucleic Acids Res.* **47**, 6488–6503 (2019).
73. B. R. Dudenhoeffer, H. Schneider, K. Schweimer, S. H. Knauer, SuhB is an integral part of the ribosomal antitermination complex and interacts with NusA. *Nucleic Acids Res.* **47**, 6504–6518 (2019).
74. M. Worbs, G. P. Bourenkov, H. D. Bartunik, R. Huber, M. C. Wahl, An extended RNA binding surface through arrayed S1 and KH domains in transcription factor NusA. *Mol. Cell* **7**, 1177–1189 (2001).
75. S. Prasch *et al*., RNA-binding specificity of *E. coli* NusA. *Nucleic Acids Res.* **37**, 4736–4742 (2009).
76. K. S. Ha, I. Toulokhonov, D. G. Vassylyev, R. Landick, The NusA N-terminal domain is necessary and sufficient for enhancement of transcriptional pausing via interaction with the RNA exit channel of RNA polymerase. *J. Mol. Biol.* **401**, 708–725 (2010).
77. K. Schweimer *et al*., NusA interaction with the α subunit of *E. coli* RNA polymerase is via the UP element site and releases autoinhibition. *Structure* **19**, 945–954 (2011).
78. X. Guo *et al*., Structural basis for NusA stabilized transcriptional pausing. *Mol. Cell* **69**, 816–827.e4 (2018).
79. M. Strauß *et al*., Transcription is regulated by NusA:NusG interaction. *Nucleic Acids Res.* **44**, 5971–5982 (2016).
80. A. Eisenmann, S. Schwarz, S. Prasch, K. Schweimer, P. Rösch, The *E. coli* NusA carboxy-terminal domains are structurally similar and show specific RNAP- and lambdaN interaction. *Protein Sci.* **14**, 2018–2029 (2005).
81. S. Prasch *et al*., Interaction of the intrinsically unstructured phage lambda N Protein with *Escherichia coli* NusA. *Biochemistry* **45**, 4542–4549 (2006).
82. T. F. Mah, K. Kuznedelov, A. Mushegian, K. Severinov, J. Greenblatt, The alpha subunit of *E. coli* RNA polymerase activates RNA binding by NusA. *Genes Dev.* **14**, 2664–2675 (2000).
83. J.-M. Choi, A. S. Holehouse, R. V. Pappu, Physical principles underlying the complex biology of intracellular phase transitions. *Annu. Rev. Biophys.* **49**, 107–133 (2020).
84. S. Elbaum-Garfinkle *et al*., The disordered P granule protein LAF-1 drives phase separation into droplets with tunable viscosity and dynamics. *Proc. Natl. Acad. Sci. U.S.A.* **112**, 7189–7194 (2015).
85. A. V. Ceballos, C. J. McDonald, S. Elbaum-Garfinkle, Methods and strategies to quantify phase separation of disordered proteins. *Methods Enzymol.* **611**, 31–50 (2018).
86. B. Monterroso *et al*., Bacterial FtsZ protein forms phase-separated condensates with its nucleoid-associated inhibitor SlmA. *EMBO Rep.* **20**, e45946 (2019).
87. J. Wang *et al*., A molecular grammar governing the driving forces for phase separation of prion-like RNA binding proteins. *Cell* **174**, 688–699.e16 (2018).
88. I. F. Lau *et al*., Spatial and temporal organization of replicating *Escherichia coli* chromosomes. *Mol. Microbiol.* **49**, 731–743 (2003).
89. S. Wang, J. R. Moffitt, G. T. Dempsey, X. S. Xie, X. Zhuang, Characterization and development of photoactivatable fluorescent proteins for single-molecule-based superresolution imaging. *Proc. Natl. Acad. Sci. U.S.A.* **111**, 8452–8457 (2014).
90. T. R. Beattie *et al*., Frequent exchange of the DNA polymerase during bacterial chromosome replication. *eLife* **6**, 22635 (2017).
91. S. Bakshi, R. M. Dalrymple, W. Li, H. Choi, J. C. Weisshaar, Partitioning of RNA polymerase activity in live *Escherichia coli* from analysis of single-molecule diffusive trajectories. *Biophys. J.* **105**, 2676–2686 (2013).
92. S. C. Weber, A. J. Spakowitz, J. A. Theriot, Bacterial chromosomal loci move subdiffusively through a viscoelastic cytoplasm. *Phys. Rev. Lett.* **104**, 238102 (2010).
93. J. D. Karslake *et al*., SMAUG: Analyzing single-molecule tracks with nonparametric Bayesian statistics. *Methods*, S1046-2023–3 (2020).
94. M. Schaechter, O. Maaloe, N. O. Kjeldgaard, Dependency on medium and temperature of cell size and chemical composition during balanced grown of *Salmonella typhimurium*. *J. Gen. Microbiol.* **19**, 592–606 (1958).
95. N. S. Shepherd, G. Churchward, H. Bremer, Synthesis and activity of ribonucleic acid polymerase in *Escherichia coli*. *J. Bacteriol.* **141**, 1098–1108 (1980).
96. H. Bremer, P. Dennis, M. Ehrenberg, Free RNA polymerase and modeling global transcription in *Escherichia coli*. *Biochimie* **85**, 597–609 (2003).
97. S. Klumpp, T. Hwa, Growth-rate-dependent partitioning of RNA polymerases in bacteria. *Proc. Natl. Acad. Sci. U.S.A.* **105**, 20245–20250 (2008).
98. M. Nomura, D. M. Bedwell, M. Yamagishi, J. R. Cole, J. M. Kolb, "RNA polymerase and regulation of rRNA synthesis in *Escherichia coli*: RNA polymerase concentration, stringent control, and ribosome feedback regulation" in *RNA Polymerase and the Regulation of Transcription*, W. S. Reznikoff, Ed. (Elsevier, New York, 1987), pp. 137–149.
99. C. P. Brangwynne, T. J. Mitchison, A. A. Hyman, Active liquid-like behavior of nucleoli determines their size and shape in *Xenopus laevis* oocytes. *Proc. Natl. Acad. Sci. U.S.A.* **108**, 4334–4339 (2011).
100. M. Feric *et al*., Coexisting liquid phases underlie nucleolar subcompartments. *Cell* **165**, 1686–1697 (2016).
101. R.-W. Yao *et al*., Nascent pre-rRNA sorting via phase separation drives the assembly of dense fibrillar components in the human nucleolus. *Mol. Cell* **76**, 767–783.e11 (2019).
102. M. Scott, C. W. Gunderson, E. M. Mateescu, Z. Zhang, T. Hwa, Interdependence of cell growth and gene expression: Origins and consequences. *Science* **330**, 1099–1102 (2010).
103. A. S. Holehouse, R. V. Pappu, Functional implications of intracellular phase transitions. *Biochemistry* **57**, 2415–2423 (2018).
104. H. Yoo, C. Triandafillou, D. A. Drummond, Cellular sensing by phase separation: Using the process, not just the products. *J. Biol. Chem.* **294**, 7151–7159 (2019).
105. R. L. Gourse *et al*., Transcriptional responses to ppGpp and DksA. *Annu. Rev. Microbiol.* **72**, 163–184 (2018).
106. A. Dönhöfer *et al*., "Factor-mediated ribosome assembly in bacteria" in *Encyclopedia of Life Sciences*, (Wiley Online Library, Chichester, 2009).
107. T. J. Nott *et al*., Phase transition of a disordered nuage protein generates environmentally responsive membraneless organelles. *Mol. Cell* **57**, 936–947 (2015).
108. L. R. Racki *et al*., Polyphosphate granule biogenesis is temporally and functionally tied to cell cycle exit during starvation in *Pseudomonas aeruginosa*. *Proc. Natl. Acad. Sci. U.S.A.* **114**, E2440–E2449 (2017).
109. R. Janissen *et al*., Global DNA compaction in stationary-phase bacteria does not affect transcription. *Cell* **174**, 1188–1199.e14 (2018).
110. F. Heinkel *et al*., Phase separation and clustering of an ABC transporter in *Mycobacterium tuberculosis*. *Proc. Natl. Acad. Sci. U.S.A.* **116**, 16326–16331 (2019).
111. B. Niewidok *et al*., Single-molecule imaging reveals dynamic biphasic partition of RNA-binding proteins in stress granules. *J. Cell Biol.* **217**, 1303–1318 (2018).
112. S. Pitchiaya *et al*., Dynamic recruitment of single RNAs to processing bodies depends on RNA functionality. *Mol. Cell* **74**, 521–533.e6 (2019).
113. K. Lasker *et al*., Selective sequestration of signalling proteins in a membraneless organelle reinforces the spatial regulation of asymmetry in *Caulobacter crescentus*. *Nat. Microbiol.* **5**, 418–429 (2020).
114. J.-Y. Tinevez *et al*., TrackMate: An open and extensible platform for single-particle tracking. *Methods* **115**, 80–90 (2017).